Arch. Metall. Mater. **71** (2026), 3, 861-872

DOI: https://doi.org/10.24425/amm.2026.1977

GRZEGORZ MOSKAL[1*]

PREDICTION OF TBC'S EFFECTIVE THERMAL CONDUCTIVITY BASED ON DFT-DERIVED MATERIAL DATA AND EXPERIMENTALLY DETERMINED MICROSTRUCTURAL PARAMETERS

This article presents research on predicting the effective thermal conductivity of single-phase thermal barrier coating insulating layers, based on DFT thermal conductivity simulations, experimentally determined microstructural (porosity) data, and knowledge of interface thermal resistance. Based on the analyses, the best agreement between predictions and actual results was observed for relationships that accounted for splat geometry and interfacial resistance. The results demonstrated a certain convergence in values and trends in temperature change over the range 25 to 1100°C. The research indicates that simulations based on DFT results and assumed splat porosity and geometry can be a useful method for designing the technological process for manufacturing TBC coatings by plasma spraying.

Keywords: TBC; thermal barrier coatings; effective thermal conductivity; prediction; DFT

1. Introduction

Thermal barrier coating (TBC) systems are an advanced solution in terms of both materials and technology. The main application area for TBCs is components exposed to high temperatures, where thermal protection of the substrate is required to maintain its high-strength properties. Such conditions typically occur in the hot sections of both aircraft and stationary gas turbines; therefore, this application area is a primary driver of development and innovation in materials and technologies for thermal barrier coatings [1-3].

The main element of the TBC system responsible for the thermal insulation effect is the outer ceramic sublayer, along with various aspects of its internal structure (i.e., thickness, pore and crack architecture, size, and splats geometry). Controlling its thermal conductivity is one of the most intensively developed issues in thermal barrier coating engineering. This can be achieved by developing new ceramic materials with a highly defective structure, a high tendency to phonon scattering, and resistance to radiative heat transfer. The second source of insulating properties is the appropriate microstructure of the ceramic layer, related to porosity and the presence of cracks, especially those oriented perpendicular to the direction of heat transfer [4-6].

A separate issue is predicting thermal conductivity in TBC systems, which is not a simple matter. This stems from the extraordinarily complex microstructure of the insulating layer, which depends on the deposition technology used (with APS and EB-PVD (atmospheric plasma spraying, electro-beam physical vapour deposition) being the dominant methods), making it very difficult to establish a correlation with thermal conductivity and not guaranteed. This stems from the fact that thermal conductivity, which accounts for various heat transport mechanisms, is influenced by factors at multiple scales – from macrostructure through microstructure to the lattice structure within the unit cell. To make this issue even more complex, it is also necessary to consider the thermal resistance of grain boundaries, which, for example, in APS-sprayed coatings, is expressed as the thermal interface resistance. Each of the above-mentioned elements strongly influences the mechanisms of heat transport and the mechanisms that generate thermal resistance, meaning that even slight changes at diverse levels of the structure can significantly affect the insulating properties [7-12].

Another significant limitation in predicting thermal effects in TBC systems is the lack of material data, such as for the ceramics used in the systems in question. This undoubtedly affects the accuracy and reliability of predictions obtained using various methods.

The literature provides a wealth of information on various methods for predicting the insulating properties of TBC systems (and, in fact, heterogeneous structures). The most widely used

[1] SILESIAN UNIVERSITY OF TECHNOLOGY, MATERIALS INNOVATION LABORATORY, 8 KRASIŃSKIEGO STR., 40-019 KATOWICE, POLAND

* Corresponding author: grzegorz.moskal@polsl.pl

is analytical modelling based on the Effective Medium Theory (EMT) [13-15], which assumes macroscale homogeneity while simultaneously assuming a heterogeneous microstructural character. EMT is a set of mathematical models within the mean-field theory group, used to describe the transport properties (electrical or thermal conductivity) of heterogeneous systems such as composites. Individual models consider the microstructural characteristics of materials, such as the volume/mass fractions of individual phases (including voids) and their spatial configuration, as well as thermal phenomena occurring between individual components of the composite (so-called interfacial resistance). Historically, the first models with practical applications were the Ohm model (series and parallel), Maxwell, Klemens, and Rayleigh models, originally used to predict electrical conductivity [16]. In these models, estimating the effective conductivity requires only knowledge of the volume fraction of the phase (e.g., pores) and the electrical or thermal conductivities of the matrix and the second phase. However, these models are effective only when the second phase (pores) is relatively small; an additional requirement is that it be spherical. Pore morphology other than spherical and higher volume fractions are considered in the Maxwell-Eucken, Maxwell-Garnet, and Lewis-Nielsen models [16-18]. This is an extremely important issue because, in TBC systems, the microstructural heterogeneity of the ceramic (insulating) layer is created by the ceramic-void system, i.e., spherical and horizontal pores (cracks), respectively. The presence of horizontal pores was accounted for in the Kachanov equation [19], which considered disc-shaped pores oriented perpendicular to the heat-flow direction and characterised by parameters such as pore length and thickness. Jadhav's combination of Maxwell's dependencies (for spherical pores) and Kachanov's dependencies (for horizontal pores) by introducing the functions describing them into the Scardi iterative model (considering various morphological forms of pores) allowed for the formulation of dependencies considering both morphological types of pores, typical for TBC systems [19-22].

These models, like the previously described basic models, do not account for phenomena at interface boundaries, which is a significant weakness [23]. Among these phenomena, interface thermal resistance (ITR) is dominant in predicting effective conductivity. It results from local discontinuities between individual phase components. The presence of thermal resistance generates a temperature jump at the interface between individual phase components due to a disturbance in the heat flux. Interface thermal resistance has two dominant components. The first is thermal contact resistance (TCR), which arises from relatively weak physical and chemical bonds between atoms in the crystal lattices of adjacent phases. Another possible source is the presence of voids or other microstructural defects in the interfacial region. The second component of interface resistance is the so-called Kapitza thermal boundary resistance (TBR). This resistance, in turn, results from differences in the physical and chemical properties of the individual phase components in the system [23-27].

Mathematical models that account for the thermal resistance of the interfacial boundary in determining the effective thermal conductivity of two-phase systems can be found in the literature [28]. These include the Hasselman-Johanson model [29,30], Benveniste and Miloh [31-34], Bruggeman [35,36], and its extension, the Every and Tzou model [37,38]. The Tavangar, Molin, and Weber model is also very interesting, as it extends the applicability of the Hasselman-Jonson model and is based on the Differential Effective Medium (DEM) method [39-41].

Due to the systematic nature of the presented review, it is also necessary to mention the prediction of effective thermal conductivity using the percolation model, which explains the rapid increase in effective thermal conductivity by creating direct heat transport "paths" through connecting areas in the composite system, with relatively higher thermal conductivity than the matrix (creating heat ducts) [42].

The above models refer to the steady-state heat transfer. In unsteady conditions, it is the thermal diffusivity, not the thermal conductivity, of the system that is important. Under such conditions, dynamic models that allow the determination of effective heat transfer properties under unsteady heat transfer are used to determine these values. Such models include the Monde and Mitsutake models, which use solutions based on inverse methods for unsteady heat transfer (Inverse Problem of One-Conditional Unsteady Heat Conduction) [43], the Salazar model [44,45], the Fang model [46], and its extension, the Fang-Hu-Wang model [47].

A completely different approach to predicting the thermal properties of TBC systems is provided by methods based on artificial intelligence, i.e. neural networks [48-50] and machine learning [51-53], which, however, is not the subject of this publication.

2. Motivation

The purpose of this article is to present analyses of the potential for predicting the effective thermal conductivity of single-phase and single-layer TBC systems based on quantitative and qualitative assessments of spherical porosity and horizontal cracks. Using DFT (Density Functional Theory) simulation results, the theoretical thermal conductivity of the ceramic phases from which the TBC systems were constructed was determined. Using the results of spherical and horizontal porosity measurements, DFT simulations, and LFA measurements of thermal diffusivity of ceramic sinters, as well as the Maxwell, Maxwell-Garnet, Maxwell-Taylor, Maxwell-Eucken, Klemens, Lewis-Nielsen, Reyleigh, Bruggeman equations, the EMT model, and the Scardi-Jadhav model, the predicted effective thermal conductivity of TBC systems with assumed porosity was determined. These values were compared with experimental results obtained from measurements of actual TBC systems. The conductivity of these systems was calculated from experimental measurements of the thermal diffusivity of two-layer systems, and the thermal diffusivity was determined using the two-layer model available in Netzsch's Proteus software [54]. In the second stage of the study, the thermal resistance of the intergrain

(inter-splat / splat-to-spalt) interface was also accounted for in the analyses. In this case, the multilayer model for ceramic coatings presented in Ravichandran [55] and the relationship that accounts for the interfacial thermal resistance (ITR) of grain boundaries presented in Smith et al. [56] were used.

A new element of the presented research is the determination of the effective thermal conductivity of TBC systems using both DFT-simulated material parameters and experimental studies of porosity, spall geometry, and thermal resistance at intersplat interfaces. Until now, DFT simulation results for TBC systems have been used to determine the parameters of ceramic materials used to fabricate the insulating layer (elastic constants, thermal conductivity as a function of temperature, and minimum thermal conductivity – a criterion value for material selection for TBCs). However, there is no literature data that allows for combining DFT simulation results with actual TBC systems with specific microstructural characteristics (porosity, thermal resistance), which is the main topic of this publication.

3. Experimental procedure

Using the DFT framework, calculations were performed with the Cambridge Serial Total Energy Simulation Package (CASTEP) code. The ion-electron interactions were modelled using Optimised Norm-Conserving Vanderbilt pseudopotentials. Geometry optimisation and relaxation techniques were employed to determine the equilibrium lattice parameters and unit cell volume. The optimised crystal structures were subsequently utilised to examine the properties of the pyrochlore compounds studied. The GGA-PBE functional was used for the electronic structure calculations, with an 830 eV energy cutoff and a 6×6×6 k-point sampling, to obtain results comparable to experimental data. The optimisation convergence criteria were set to 0.01 eV/Å for interatomic forces, 5×10^{-6} eV for total energy, 2×10^{-2} GPa for stress, and 5×10^{-4} Å for maximum ionic displacement [57,58].

The studies were conducted on five TBC systems: a conventional system based on the compound 8YSZ ($8Y_2O_3\times ZrO_2$ – wt.%) and systems based on new ceramic materials for TBCs, i.e., $La_2Zr_2O_7$, $Nd_2Zr_2O_7$, $Sm_2Zr_2O_7$, and $Gd_2Zr_2O_7$. The coatings were produced by air plasma spraying (APS). The substrate material was an IN-625 nickel superalloy with a NiCrAlY interlayer. The interlayer was also produced by the APS method and was characterized by a thickness of 125 μm. The thickness of the ceramic layer, depending on the coating type, ranged from 200 to 300 μm. A detailed description of the microstructure of the analyzed TBC systems, with particular emphasis on the ceramic layer and its morphology, was presented in previous publications [59-64]. The results of porosity tests obtained using ImageJ FiJi software [65] are presented in TABLE 1. The measurement was performed on 25 SEM images. The results of DFT simulations determining the values of theoretical thermal conductivity (used in subsequent calculations), density, and heat capacity are presented in TABLE 2 (a detailed methodological description, as well as the results of these analyses, are the subject of a separate publication [66]). TABLE 3 presents the results of experimental

TABLE 1

Results of quantitative and qualitative analysis of porosity

TBC system	Stereological parameter	Overall porosity	Spherical porosity	Horizontal porosity	Vertical porosity
$8Y_2O_3\times ZrO_2$	φ [%]	9,74 ± 0,23	2,54 ± 0,07	7,17 ± 0,17	0,03 ± 0,001
$La_2Zr_2O_7$	φ [%]	3,65 ± 0,09	2,53 ± 0,07	1,10 ± 0,03	0,03 ± 0,001
$Nd_2Zr_2O_7$	φ [%]	4,40 ± 0,11	2,07 ± 0,06	2,31 ± 0,04	0,02 ± 0,001
$Sm_2Zr_2O_7$	φ [%]	2,83 ± 0,07	1,81 ± 0,05	1,00 ± 0,02	0,01 ± 0,001
$Gd_2Zr_2O_7$	φ [%]	4,50 ± 0,12	1,52 ± 0,05	2,93 ± 0,05	0,05 ± 0,001

TABLE 2

Results of DFT simulations of thermal conductivity

Temperature °C	$8Y_2O_3\times ZrO_2$	$La_2Zr_2O_7$	$Nd_2Zr_2O_7$	$Sm_2Zr_2O_7$	$Gd_2Zr_2O_7$
	Theoretical thermal conductivity – Slack equation W/mK				
25	7,111	3,667	3,017	3,998	3,348
100	5,324	2,746	2,259	2,994	2,507
200	4,255	2,194	1,805	2,393	2,004
300	3,544	1,827	1,504	1,993	1,669
400	3,036	1,566	1,288	1,707	1,429
500	2,656	1,369	1,127	1,493	1,250
600	2,360	1,217	1,001	1,327	1,111
700	2,123	1,095	0,901	1,194	1,000
800	1,930	0,995	0,819	1,085	0,909
900	1,769	0,912	0,751	0,995	0,833
1000	1,633	0,842	0,693	0,918	0,769
1100	1,516	0,782	0,643	0,852	0,714

TABLE 3

Results of thermal diffusivity of sinters measurement by the LFA method

Temperature °C	$8Y_2O_3{\times}ZrO_2$	$La_2Zr_2O_7$	$Nd_2Zr_2O_7$	$Sm_2Zr_2O_7$	$Gd_2Zr_2O_7$
	Experimental thermal diffusivity mm^2/s				
25	2,74 ± 0,08	1,78 ± 0,05	1,70 ± 0,06	1,51 ± 0,05	1,30 ± 0,03
100	2,39 ± 0,07	1,45 ± 0,04	1,44 ± 0,05	1,32 ± 0,04	1,14 ± 0,02
200	2,15 ± 0,06	1,31 ± 0,04	1,26 ± 0,03	1,15 ± 0,03	1,04 ± 0,01
300	1,93 ± 0,04	1,23 ± 0,03	1,14 ± 0,02	1,04 ± 0,02	0,97 ± 0,01
400	1,73 ± 0,04	1,15 ± 0,03	1,06 ± 0,02	1,02 ± 0,02	0,91 ± 0,01
500	1,51 ± 0,03	1,09 ± 0,02	1,01 ± 0,01	0,97 ± 0,01	0,87 ± 0,01
600	1,38 ± 0,03	1,05 ± 0,02	0,96 ± 0,01	0,92 ± 0,01	0,83 ± 0,01
700	1,31 ± 0,03	1,00 ± 0,01	0,95 ± 0,01	0,90 ± 0,01	0,82 ± 0,01
800	1,26 ± 0,03	0,95 ± 0,01	0,90 ± 0,01	0,90 ± 0,01	0,81 ± 0,01
900	1,28 ± 0,03	0,93 ± 0,01	0,89 ± 0,01	0,88 ± 0,01	0,80 ± 0,01
1000	1,31 ± 0,04	0,96 ± 0,01	0,90 ± 0,01	0,92 ± 0,01	0,82 ± 0,01
1100	1,43 ± 0,04	1,00 ± 0,01	0,91 ± 0,01	0,91 ± 0,01	0,85 ± 0,01

measurement of thermal diffusivity of sinters using the LFA method. In this case, the measurement accuracy was 3%. The values of heat capacity and theoretical density, also obtained based on DFT simulations, are presented in TABLE 4. TABLE 5 presents a summary of the mathematical relationships used in the prediction of effective thermal conductivity and the type of output data – thermal conductivity determined based on DFT simulations and the LFA method.

The results of effective thermal conductivity calculations based on these relationships were compared with the thermal conductivity of TBC systems fabricated for this study, which were determined based on experimental measurements of thermal diffusivity over a temperature range of 25-1100°C (using a Netzsch LFA 427 analyzer) and heat capacity and density determined by DFT.

Thermal conductivity was calculated as the product of these three parameters. As an alternative to DFT simulations, thermal diffusivity and thermal conductivity were also determined for 8YSZ, $La_2Zr_2O_7$, $Nd_2Zr_2O_7$, $Sm_2Zr_2O_7$, and $Gd_2Zr_2O_7$ sinters, which were used in the calculations of effective thermal conductivity for the Scardi-Jadhav relationships, the layered model, and the ITR models.

TABLE 4

Results of DFT simulations of thermal conductivity

Temperature °C	$8Y_2O_3{\times}ZrO_2$	$La_2Zr_2O_7$	$Nd_2Zr_2O_7$	$Sm_2Zr_2O_7$	$Gd_2Zr_2O_7$
Specific heat J/gK	0.428	0.405	0.402	0.401	0.375
Density kg/m^3	6150	5995	6272	6510	6760

TABLE 5

The functional relationship used in the presented analysis to calculate effective thermal conductivity

Relationship name	Equation	λ_{solid} value source
1	2	3
Ohm parallel	$\lambda_{eff} = \phi_{sph}\lambda_{por} + \left(1-\phi_{sph}\right)\lambda_{solid}$	λ_{solid} – LFA
Maxwell	$\lambda_{eff} = \left(1-\frac{3\phi_{sph}}{2}\right)\lambda_{solid}$	λ_{solid} – LFA
Klemens	$\lambda_{eff} = \left(1-\frac{4\phi_{sph}}{3}\right)\lambda_{solid}$	λ_{solid} – LFA
Maxwell-Taylor	$\lambda_{eff} = 1-\left[\frac{3\phi_{sph}(1-\lambda_{por}/\lambda_{solid})}{2+\lambda_{por}/\lambda_{solid}}\right]\lambda_{solid}$	λ_{solid} – LFA
Maxwell-Garnett	$\lambda_{eff} = \lambda_{solid}\left[\frac{\lambda_{por}\left(1+\left(2\phi_{sph}\right)\right)-\lambda_{solid}\left(2\phi_{sph}-2\right)}{\lambda_{solid}\left(2+\phi_{sph}\right)+\left(\lambda_{por}\left(1-\phi_{sph}\right)\right)}\right]$	λ_{solid} – LFA

TABLE 5. Continued

1	2	3
Maxwell-Eucken	$\lambda_{eff} = \lambda_{solid}\left(\frac{2\lambda_{solid}+\lambda_{por}-2\left(\lambda_{solid}-\lambda_{por}\right)\phi_{sph}}{2\lambda_{solid}+\lambda_{por}+\left(\lambda_{solid}-\lambda_{por}\right)\phi_{sph}}\right)$	λ_{solid} – LFA
Rayleigh	$1-\phi_{sph}=\frac{\lambda_{eff}/\lambda_{solid}-\lambda_{por}/\lambda_{solid}}{\left(\lambda_{eff}/\lambda_{solid}\right)^{1/3}\left(1-\lambda_{por}/\lambda_{solid}\right)}$	λ_{solid} – LFA
Lewis-Nielsen	$\lambda_{eff} = \lambda_{solid}\left(1+\left(AB\phi_{sph}\right)/\left(1-\left(B\psi\phi_{sph}\right)\right.\right.$	λ_{solid} – LFA
EMT	$\lambda_{eff} = 0.25\left[\left(\lambda_{por}\left(3\phi_{sph}-1\right)+\lambda_m\left(3(1-\phi_{sph}\right))-1\right)\right]+$ $+\left\{\left[\left(\lambda_{por}\left(3\phi_{sph}-1\right)+\left(3\left(1-\phi_{sph}\right)-1\right)\right)\lambda_{solid}\right]^2+8\lambda_{solid}\lambda_{por}\right\}^{1/2}$	λ_{solid} – LFA
Scardi-Jadhav	$\lambda_{eff}=\frac{1}{2}\lambda_{solid}\left[f_2\left(\frac{\phi_{hor}}{1-\phi_{sph}}\right)\cdot f_1\left(\phi_{sph}\right)+f_1\left(\frac{\phi_{sph}}{1-\phi_{hor}}\right)\cdot f_2\left(\phi_{hor}\right)\right]$	λ_{solid} – LFA, DFT
Layered model	$\lambda_{eff}=1/\left(\left(\frac{1}{\lambda_{solid}}+\frac{n-1}{Lh_c}\right)\right.$	λ_{solid} – DFT
ITR model	$\lambda_{eff}=1/\left(\left(\frac{1}{\lambda_{solid}}+nR_{\text{int}}\right)\right.$	λ_{solid} – DFT

where: λ_{solid} – thermal conductivity of solid matrix, λ_{por} – thermal conductivity of pores, λ_{eff} – effective thermal conductivity, ϕ_{sph} – spherical porosity, ϕ_{hor} – horizontal porosity, n – number of splats/grains, L – thickness of ceramic layer, R_{int} – thermal resistance of interface ($1/h_c$).

4. Results

The calculated thermal conductivity results of the tested thermal barrier coatings, obtained as the product of experimentally measured thermal diffusivity, heat capacity, and density determined by DFT simulation (TABLE 4), are presented in Fig. 1. These data indicate that the best insulating properties were exhibited by TBC systems based on new ceramic materials with pyrochlore-type networks, i.e., lanthanum, neodymium, samarium, and gadolinium zirconates. This observation applies

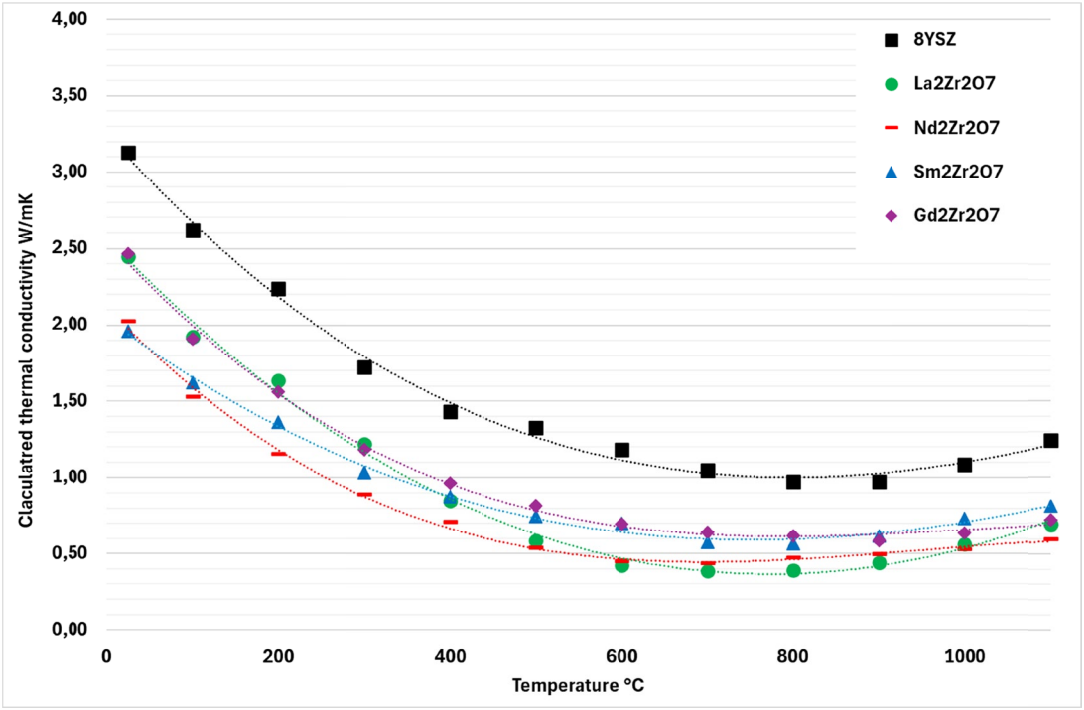

Fig. 1. Computational result of thermal conductivity of the tested TBC systems based on direct measurements of thermal diffusivity

to the entire temperature range of the measurement. The nature of the thermal conductivity changes in the tested materials is typical for ceramic phases, where the thermal resistance effect results from various phonon scattering mechanisms (e.g., the Um-klapp process). This is evidenced, for example, by the inverse-proportional decrease in thermal conductivity ($\lambda \sim f(1/T)$) as temperature increases. This decrease is observed up to approximately 700°C, above which the radiative heat transport mechanism also plays a significant role.

These values served as a reference point for calculations regarding the prediction of thermal conductivity of TBC systems based on knowledge of thermal diffusivity or thermal conductivity of solid materials, e.g., thermal diffusivity of sinters made of materials analogous to TBC systems or thermal conductivity values determined using DFT simulations. These data are presented in TABLES 2 and 3. The results of spherical and horizontal porosity tests, presented in TABLE 1, were also used for the calculations. A summary of the relationships that enable the computational determination of the effective thermal conductivity of the tested ceramic layers is presented in TABLE 5, and the calculation results obtained from these relationships are shown in Fig. 2.

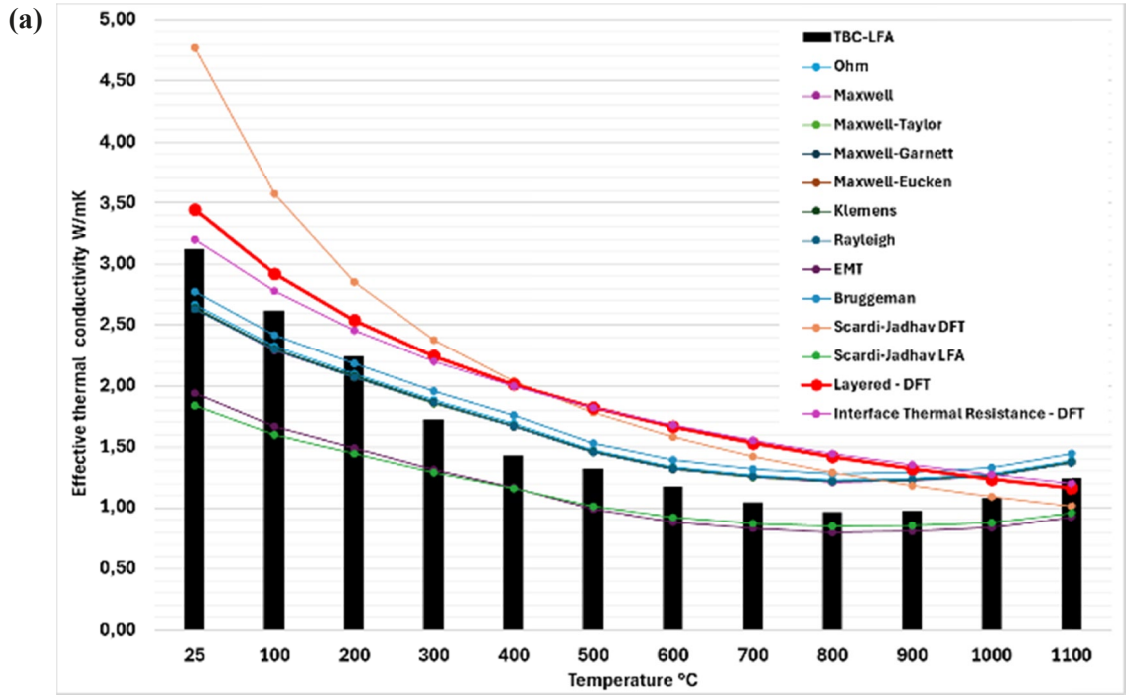

8YSZ

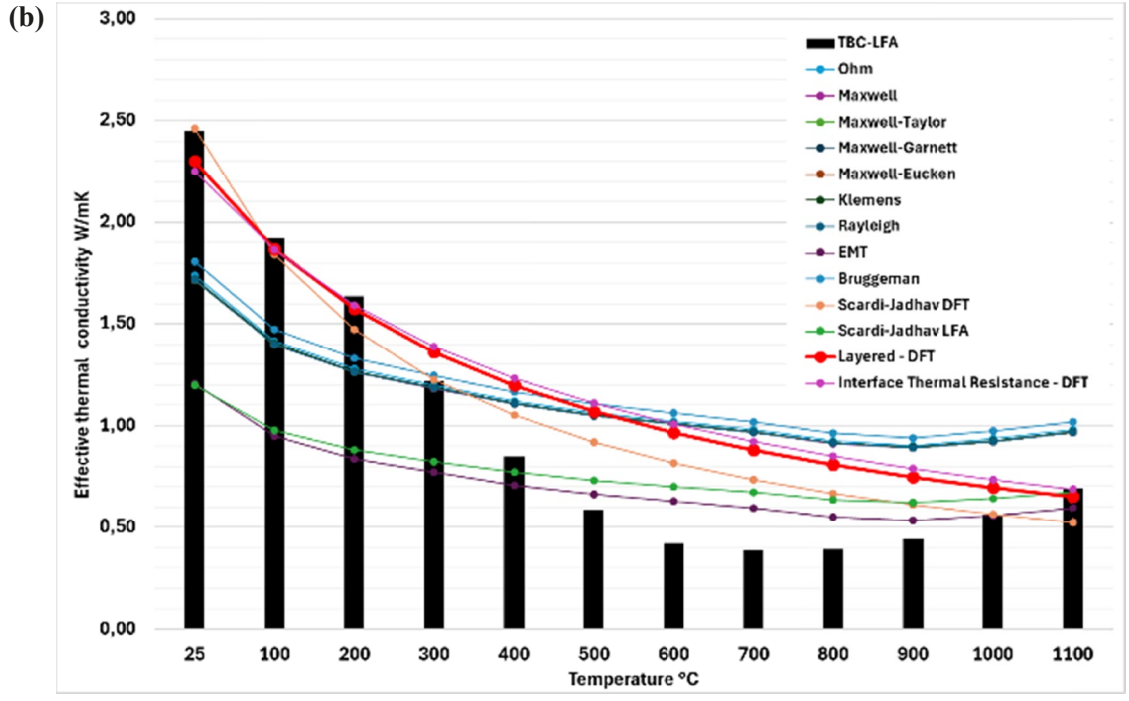

$La_2Zr_2O_7$

The data presented in Fig. 2 show that the results of the predictions of effective thermal conductivity obtained on the basis of DFT simulation data and experimental measurements of microstructural parameters (porosity and slat geometry with a measurement uncertainty of about 2 to 3%) are close to the results of experimental measurements for real TBC systems, determined on the basis of thermal diffusivity measurements (with a measurement uncertainty of about 3.5%). This is particularly true for the layered model, modified to a single-layer system, in which the individual layers correspond to the weave thicknesses obtained during APS spraying of the ceramic layer. An equally precise match was obtained for the ITR model used for sintered materials.

It should be noted that the interface thermal conductivity of 7.76×10^5 W/m^{2}K was used in the calculations, a value determined in [11]. The thermal resistance value used in the calculations is the average over the temperature range 25-1100°C, determined from laser flash measurements for systems based on La, Nd, Sm, and Gd zirconates. The differences in thermal resistance values between the individual types of materials were

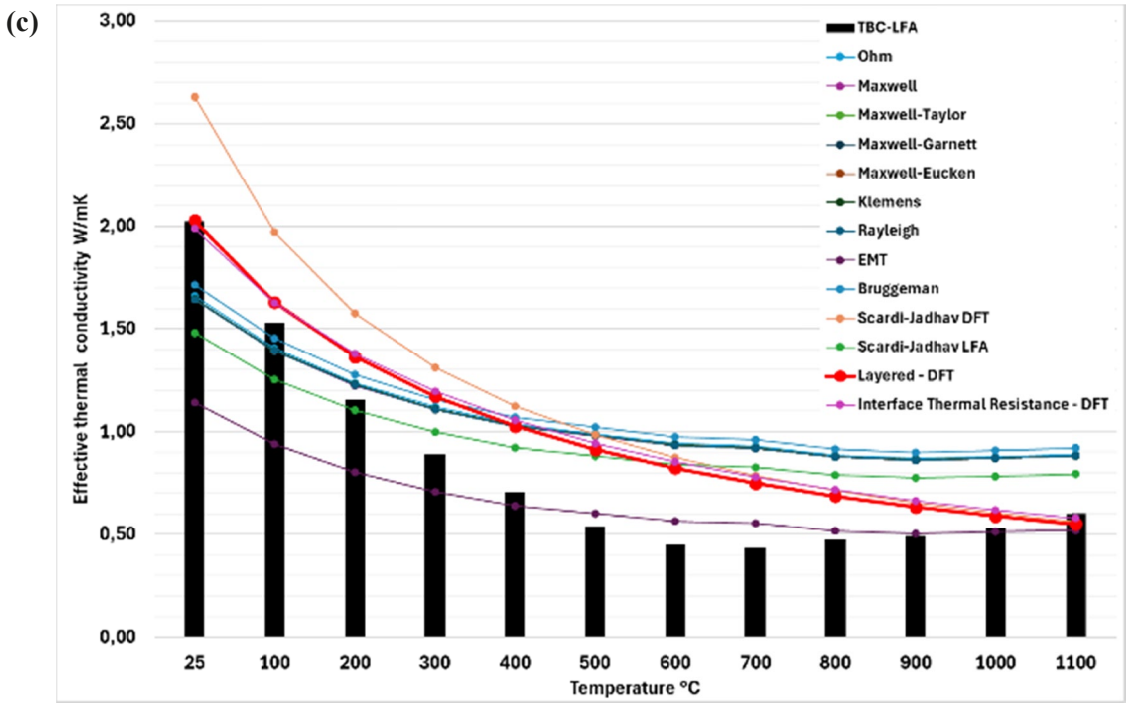

$Nd_2Zr_2O_7$

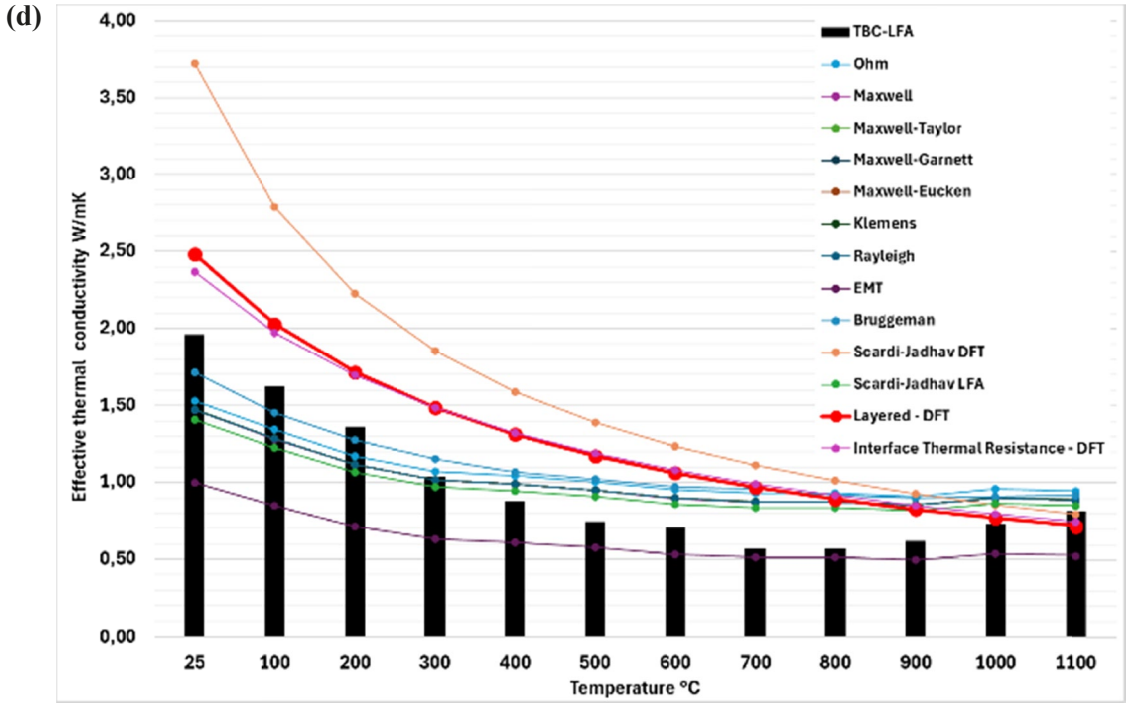

$Sm_2Zr_2O_7$

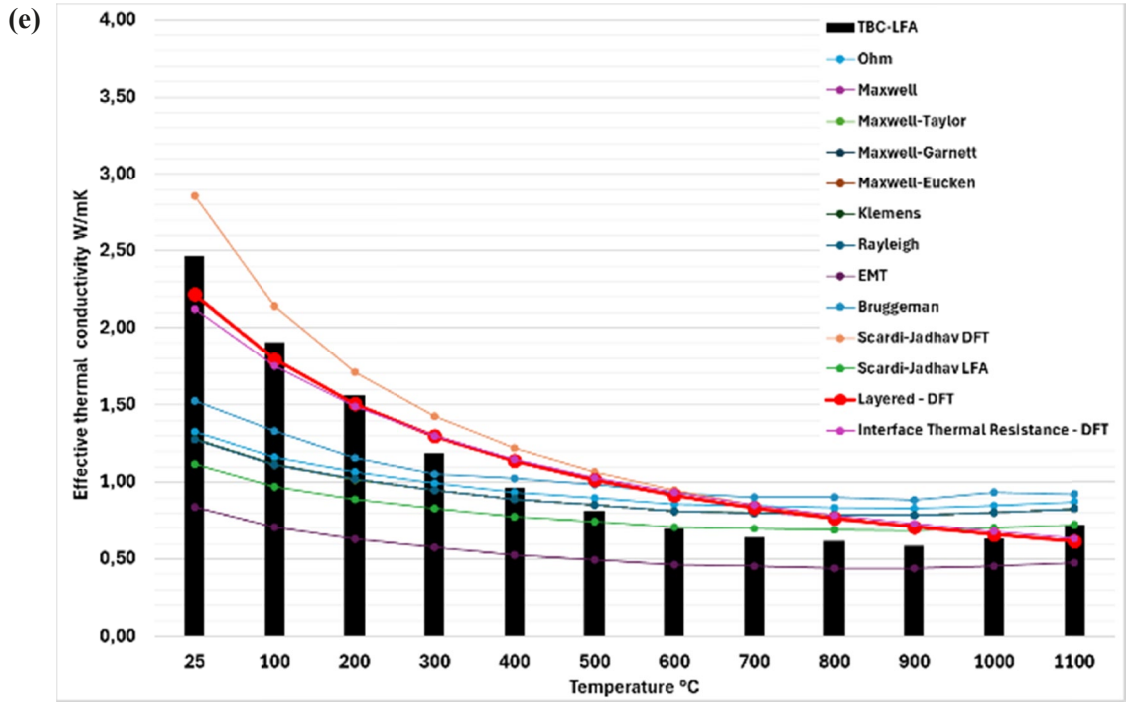

$Gd_2Zr_2O_7$

Fig. 2(a-e). Summary of calculation results of effective thermal conductivity of TBC systems

small, and the error value expressed as standard deviation did not exceed 4.5%. In some cases, the Scardi-Jadhav model was also effective, with DFT simulation results entered as thermal conductivity values. This is especially true for the $La_2Zr_2O_7$-based TBC system. The relatively best fit of all models using the values obtained in DFT simulations was noted for the $Gd_2Zr_2O_7$ coating, and the largest differences with the experimentally measured values were observed for the $Sm_2Zr_2O_7$ type TBC coatings.

5. Summary

The DFT (density functional theory) method, like other ab initio methods, enables the determination of fundamental physical parameters of materials, including components of the stress tensor. This allows for the determination of theoretical values of elastic moduli, including Young's modulus, which is the basis for determining the speed of sound in a given crystal lattice – in effect, the velocity of phonon wave propagation, which corresponds to the thermal conductivity of a crystal with a specific lattice type. Using Cahill or Clark relations, it is possible to determine the minimum thermal conductivity of such crystals, a criterion value for selecting materials for insulating applications, such as TBC systems. The Slack relation, in turn, allows for the determination of the dependence of phonon conductivity on temperature. Indeed, these values refer to crystals with an ideal lattice structure.

In the case of real TBC systems obtained by APS plasma spraying, we deal with splat-to-splat boundaries, a defined splat geometry (thickness and width), specific interface morphology, and spherical, horizontal, and vertical porosity.

For interphase boundaries in sintered materials, studies presented in [67] showed that the resistance of the $Y_2O_3{\times}ZrO_2$/$Y_2O_3{\times}ZrO_2$ interface was $4.5{\times}10^{-9}$ m^2 KW^{-1}, while for the Al_2O_3/Al_2O_3 interface it was $0.9\text{-}1.3{\times}10^{-8}$ m^2 KW^{-1} [68,69]. These values are low enough not to significantly affect the results of theoretical calculations that account for thermal resistance. However, it is assumed that the thermal resistance of a heterogeneous interface is higher than that of homonymous interfaces in single-phase materials. The increased resistance in two-phase materials may result from differences in the coefficient of thermal expansion, which can cause mechanical defects at the interface or lead to separation of the two surfaces [70].

The situation is different for ceramic materials, which undergo consolidation by methods other than sintering. Examples of such systems include thermal insulation coatings applied by plasma spraying. When analyzing the morphology of thermal insulation coatings obtained by plasma spraying, it should be noted that a splat-to-splat interface is formed during the coating formation process. Not all splats are permanently bonded, which increases the total area of discontinuity, reducing the system's thermal conductivity. The actual bonding area between individual splats is assumed to be approximately 20%. Porosity and interlayer contact area are two key factors influencing coating properties [71-73]. All these elements limit phonon wave propagation and generate thermal resistance, thereby reducing thermal conductivity.

Therefore, using material parameters obtained from DFT simulations with relationships describing the influence of microstructural parameters such as spherical and horizontal porosity, splat width and thickness, and inter-splat boundary thermal resistance should enable relatively accurate prediction of the

thermal conductivity of TBC systems characterized by the type of material used (DFT simulations) and the microstructural characteristics of the insulating layer (spherical and horizontal porosity, splat thickness and width, number of splat-to-splat boundaries, and thickness of the ceramic coating). The main limitation in using DFT simulation results for this type of calculation is the accuracy of the results, which in turn depends on the correctness of the assumptions about the material's unit cell structure.

The studies demonstrated that first-principles simulations, including DFT calculations, can effectively predict the effective thermal conductivity of the ceramic layer in thermal barrier coatings. The best-fitting results were obtained for models that account for interface thermal resistance or its inverse, i.e., interfacial thermal conductivity, i.e. the Scardi-Jadhav model, and especially for the layered and ITR models.

In the case of the Scardi-Jadhav model, the poor fit of the results to the experimental data is related to the geometric parameters of the coating's structural elements, i.e., splat thickness and diameter. Accurate detection, closely related to the preparation of TBC systems, is a key factor in predicting efficiency. The layered and ITR models only refer to the number of splats/grains and the thermal resistance values of the interfacial boundaries and are therefore less susceptible to errors associated with revealing the splat or grain geometry. This is why the prediction results for the $Sm_2Zr_2O_7$ coating deviate from the expected accuracy. Nevertheless, in the remaining four cases, the comparison of experimental results and modelling studies is very satisfactory.

Introducing the interfacial resistance effect into the equations for determining effective thermal conductivity, along with data obtained from DFT simulations, is ineffective for the basic equations, i.e., those listed in TABLE 5, from Ohm's equation to EMT. The predictions differ significantly from the actual thermal conductivity measurements of the tested TBC systems (these measurements were not included in Fig. 1 for clarity). This is due to the absence of a component related to the interface's thermal resistance. However, using data from direct measurements of the diffusivity/thermal conductivity of sinters obtained by the LFA method in these equations allows for a good prediction of the effective thermal conductivity at ambient temperature.

6. Conclusions

Compiling functional relationships that describe the value of effective thermal conductivity from material data obtained using the DFT method enables accurate prediction of this parameter for TBC systems.

Critical factors determining the accuracy of the results include, on the one hand, correctly performed DFT simulations and, on the other hand, the precise determination of microstructural parameters of the ceramic layer, such as spherical and horizontal porosity, the number of strands/grains, and their geometry.

Effectively utilizing the microstructural design capabilities of ceramic layers in TBC systems also requires precise knowledge of the thermal resistance of the interstrand interface.

The introduction of additional data from DFT simulations (DFT) enables expanded predictions of the insulating properties of TBC systems, for example, as a function of temperature. Above all, however, it enables theoretical verification of the thermal conductivity of TBC systems based on new materials during the design phase, with significant economic implications

Acknowledgments

The research presented in this article was financed within the statutory work of the Laboratory of Material Innovations of the Silesian University of Technology No. 11/100/BK_26/0002; (BK-297/RML1/2026) and pro-quality grants of the Rector of the Silesian University of Technology No. 11/100/SDU/10-04-01 (G. Moskal).

REFERENCES

[1] D. Chellaganesh, M.A. Khan, J.W. Jappes, Thermal barrier coatings for high temperature applications – a short review. Mater. Today-Proc. **45**, 1529-1534 (2021).
DOI: https://doi.org/10.1016/j.matpr.2020.08.017

[2] K. Mondal, L. Nuñez III, C.M. Downey, I.J. Van Rooyen, Thermal barrier coatings overview: Design, manufacturing, and applications in high-temperature industries. Ind. Eng. Chem. Res. **60**, 6061-6077 (2021).
DOI: https://doi.org/ 10.1021/acs.iecr.1c00788

[3] R. Darolia, Thermal barrier coatings technology: critical review, progress update, remaining challenges and prospects. Int. Mater. Rev. **58**, 315-348 (2013).
DOI: https://doi.org/10.1179/1743280413y.0000000019

[4] G. Moskal, Selection of low and ultra-low thermal conductivity materials for insulating layers of TBC systems in the context of computational materials science opportunities – a review. J. Therm. Anal. Calorim. **150**, 7207-7251 (2025).
DOI: https://doi.org/ 10.1007/s10973-025-14226-4

[5] S.M. Lakiza, M.I. Grechanyuk O.K., Ruban, V.P. Redko, M.S. Glabay, O.B. Myloserdov, O.V. Dudnik, S.V. Prokhorenko, Thermal barrier coatings: current status, search, and analysis. Powder. Metall. Met. C+. **57**, 82-113 (2018).
DOI: https://doi.org/10.1007/s11106-018-9958-0

[6] C. Monachon, L. Weber, C. Dames, Thermal boundary conductance: A materials science perspective. Ann. Rev. Mater. Res. **46**, 433-463 (2016).
DOI: https://doi.org/10.1146/annurev-matsci-070115-031719

[7] M. Zeraati, A.R. Oganov, T. Fan, S.F. Solodovnikov, Searching for low thermal conductivity materials for thermal barrier coatings: A theoretical approach. Phys. Rev. Mater. **8**, 033601. (2024).
DOI: https://doi.org/10.1103/physrevmaterials.8.033601

[8] L. Swadźba, G. Moskal, B. Mendala, M. Hetmańczyk, Characterization of microstructure and properties of TBC systems with gradient of chemical composition and porosity. Arch. Metall. Mater. **53**, 945-954 (2008).

[9] E.P. Busso, L. Wright, H.E. Evans, L.N. McCartney, S.R.J. Saunders, S. Osgerby, J. Nunn, A physics-based life prediction metho–dology for thermal barrier coating systems. Acta. Mater. **55**, 1491-1503 (2007). DOI: https://doi.org/10.1016/j.actamat.2006.10.023

[10] M. Mikuśkiewicz, B. Witala, M. Stopyra, I. Moskal, O. Fabrichnaya, G. Moskal, The $(RE^1_{0.5}RE^2_{0.5})_2Zr_2O_7$ zirconates as a promising thermal insulating material dedicated to high-temperature applications. J. Power. Sources. **653**, 237742 (2025). DOI: https://doi.org/10.1016/j.jpowsour.2025.237742

[11] G. Moskal, M. Mikuśkiewicz, B. Witala, M. Mrówka, K. Nowińska, J. Ludew, K. Kuliński, I. Moskal, M. Gałkowska, A. Dudek, S. Roskosz, J. Zdunek, Splat-to-splat heat transfer coefficient determination in dual-phase $Ln_2Zr_2O_7$+ 8 wt% Y_2O_3× ZrO_2 thermal barrier coatings. J. Power. Sources. **660**, 238541 (2025). DOI: https://doi.org/10.1016/j.jpowsour.2025.238541

[12] G. Moskal, A. Jasik, M. Mikuśkiewicz, S. Jucha, Thermal resistance determination of $Sm_2Zr_2O_7$+ 8YSZ composite type of Tbc. Appl. Surf. Sci. **515**, 145998 (2020). DOI: https://doi.org/10.1016/j.apsusc.2020.145998

[13] T.C. Choy, Effective medium theory: principles and applications. Oxford University Press (2015).

[14] M.A. Almomani, J.A Hamdan, A Novel Approach for Adjusting the Maxwell Eucken Model and Effective Medium Theory in Computing the Thermal Conductivity of Yttria Stabilized Zirconia Thermal Barrier Coating. Jordan J. Mech. Ind. Eng. **20**, 49-58 (2026). DOI: https://doi.org/10.59038/jjmie/200105

[15] L. Gong, Y. Wang, X. Cheng, R. Zhang, H. Zhang, A novel effective medium theory for modelling the thermal conductivity of porous materials. Int. J. Heat. Mass. Tran. **68**, 295-298 (2014). DOI: https://doi.org/10.1016/j.ijheatmasstransfer.2013.09.043

[16] Y. Hirata, Thermal conduction model of metal and ceramics. Ceram. Int. **35**, 3259-3268 (2009). DOI: https://doi.org/10.1016/j.ceramint.2009.05.026

[17] D.S. Smith, A. Alzina, J. Bourret, B. Nait-Ali, F. Pennec, N. Tessier-Doyen, K. Otsu, H. Matsubara, P. Elser, U.T. Gonzenbach, Thermal conductivity of porous materials. J. Mater. Res. **28**, 2260-2272 (2013). DOI: https://doi.org/10.1557/jmr.2013.179

[18] S. Islam, G. Bhat, A model for predicting thermal conductivity of porous composite materials. Heat. Mass. Transfer. **59**, 2023-2034 (2023). DOI: https://doi.org/10.1007/s00231-023-03380-w

[19] M. Kachanov, Heat Conduction in Ceramic Coatings: Relationship Between Microstructure and Effective Thermal Conductivity. NASA/CR-1998-208200 (1998).

[20] A.D. Jadhav, N.P. Padture, E.H. Jordan, M. Gell, P. Miranzo, E.R. Fuller Jr, Low-thermal-conductivity plasma-sprayed thermal barrier coatings with engineered microstructures. Acta. Mater. **54**, 3343-3349 (2026). DOI: https://doi.org/10.1016/j.actamat.2006.03.024

[21] P. Scardi, M. Leoni, F. Cernuschi, A. Figari, Microstructure and heat transfer phenomena in ceramic thermal barrier coatings. J. AM. CERAM. SOC. **84**, 827-835 (2001). DOI: https://doi.org/10.1111/j.1151-2916.2001.tb00748.x

[22] F. Cernuschi, S. Ahmaniemi, P. Vuoristo, T. Mäntylä, Modelling of thermal conductivity of porous materials: application to thick thermal barrier coatings. J. Eur. Ceram. Soc. **24**, 2657-2667 (2004). DOI: https://doi.org/10.1016/j.jeurceramsoc.2003.09.012

[23] J. Chen, X. Xu, J. Zhou, B. Li, Interfacial thermal resistance: Past, present, and future. Rev. Mod. Phys. **94**, 025002 (2022). DOI: https://doi.org/10.1103/revmodphys.94.025002

[24] L. Wang, X.H. Zhong, Y.X. Zhao, J.S. Yang, S.Y. Tao, W. Zhang, X.G. Sun, Effect of interface on the thermal conductivity of thermal barrier coatings: A numerical simulation study. Int. J. Heat. Mass. Tran. **79**, 954-967 (2014). DOI: https://doi.org/10.1016/j.ijheatmasstransfer.2014.08.088

[25] W.B. Yuan, N. Yu, L.Y. Li, Y. Fang, Heat transfer analysis in multilayered materials with interfacial thermal resistance. Compos. Struct. **293**, 115728 (2022). DOI: https://doi.org/10.1016/j.compstruct.2022.115728

[26] D. Josell, J.E. Bonevich, T.M. Nguyen, R.N. Johnson, Heat transfer through nanoscale multilayered thermal barrier coatings at elevated temperatures. SURF. Coat. Tech. **275**, 75-83 (2015). DOI: https://doi.org/10.1016/j.surfcoat.2015.05.036

[27] S.O. Afolabi, I.O. Malachi, A.O. Olawumi, Multiscale modeling and optimization of thermal barrier coatings for interface conditions. Colloid. Surface. A. **725**, 137658 (2025). DOI: https://doi.org/10.1016/j.colsurfa.2025.137658

[28] K. Pietrak, T.S. Wiśniewski, A review of models for effective thermal conductivity of composite materials. J. Power. Technol. **95** 14-24 (2015). https://papers.itc.pw.edu.pl/index.php/JPT/article/view/463

[29] D.P.H. Hasselman, K.Y. Donaldson, J.R. Thomas Jr, Effective thermal conductivity of uniaxial composite with cylindrically orthotropic carbon fibers and interfacial thermal barrier. J. Compos. Mater. **27**, 637-644 (1993). DOI: https://doi.org/10.1177/002199839302700605

[30] D.P.H. Hasselman, Thermal diffusivity and conductivity of composites with interfacial thermal contact resistance. In Thermal Conductivity 20, Boston, MA: Springer US (1987).

[31] Y. Benveniste, Effective thermal conductivity of composites with a thermal contact resistance between the constituents: Nondilute case. J Appl. Phys. **61**, 2840-2843 (1987). DOI: https://doi.org/10.1063/1.337877

[32] Y. Benveniste, On the effective thermal conductivity of multiphase composites. Z. Angew. Math. Phys. **37**, 696-713 (1986). DOI: https://doi.org/10.1007/bf00947917

[33] Y. Benveniste, T. Miloh, The effective conductivity of composites with imperfect thermal contact at constituent interfaces. Int. J. Eng. Sci. **24**, 1537-1552 (1986). DOI: https://doi.org/10.1016/0020-7225(86)90162-x

[34] T. Miloh, Y. Benveniste, A generalized self-consistent method for the effective conductivity of composites with ellipsoidal inclusions and cracked bodies. J. Appl. Phys. **63**, 789-796 (1998). DOI: https://doi.org/10.1063/1.340071

[35] J. Ordóñez-Miranda, J.J. Alvarado-Gil, R. Medina-Ezquivel, Generalized Bruggeman formula for the effective thermal con-

ductivity of particulate composites with an interface layer. Int. J. Thermophys. **31**, 975-986 (2010).
DOI: https://doi.org/10.1016/j.mtcomm.2021.102283

[36] V.R. Raghavan, H. Martin, Modelling of two-phase thermal conductivity. Chem. Eng. Process. Process. Intensif. **34**, 439-446 (1995). DOI: https://doi.org/10.1016/0255-2701(94)00577-x

[37] D.Y. Tzou, A universal model for the overall thermal conductivity of porous media. J. Compos. Mater. **25**, 1064-1084 (1991). DOI: https://doi.org/10.1177/002199839102500806

[38] A.G. Every, Y. Tzou, D.P.H. Hasselman, R. Raj, The effect of particle size on the thermal conductivity of ZnS/diamond composites. Acta. Metall. Mater. **40**, 123-129 (1992).
DOI: https://doi.org/10.1016/0956-7151(92)90205-s

[39] R. Tavangar, J.M. Molina, L. Weber, Assessing predictive schemes for thermal conductivity against diamond-reinforced silver matrix composites at intermediate phase contrast. Scripta. Mater. **56**, 357-360 (2007).
DOI: https://doi.org/10.1016/j.scriptamat.2006.11.008

[40] R. Tavangar, L. Weber, Silver-based diamond composites with highest thermal conductivity. Emerg. Mater. Res. **1**, 67-74 (2012). DOI:https://doi.org/10.1680/emr.11.00020

[41] L. Weber, R. Tavangar, On the influence of active element content on the thermal conductivity and thermal expansion of Cu–X (X= Cr, B) diamond composites. Scripta. Mater. **57**, 988-991 (2007). DOI: https://doi.org/10.1016/j.scriptamat.2007.08.007

[42] B. Ghanbarian, H. Daigle, Thermal conductivity in porous media: Percolation-based effective-medium approximation. Water. Resour. Res. **52**, 295-314 (2016).
DOI: https://doi.org/10.1002/2015wr017236

[43] M. Monde, Y. Mitsutake, A new estimation method of thermal diffusivity using analytical inverse solution for one-dimensional heat conduction. Int. J. Heat. Mass. Tran. **44**, 16, 3169-3177 (2001). DOI: https://doi.org/10.1016/s0017-9310(00)00342-2

[44] A. Salazar, On thermal diffusivity. Eur. J. Phys. **24**, 351-358 (2003). DOI: https://doi.org/10.1088/0143-0807/24/4/353

[45] A. Salazar, J.M. Terron, A. Sánchez-Lavega, R. Celorrio, On the effective thermal diffusivity of fiber-reinforced composites. Appl. Phys. Lett. **80**, 1903-1905 (2002).
DOI: https://doi.org/10.1063/1.1461422

[46] W.Z. Fang, H. Zhang, L. Chen, W.Q. Tao, Numerical predictions of thermal conductivities for the silica aerogel and its composites. Appl. Therm. Eng. **115**, 1277-1286 (2017).
DOI: https://doi.org/10.1016/j.applthermaleng.2016.10.184

[47] X.Q. Fang, X.H. Wang, C. Hu, W.H. Huang, Nonsteady effective thermal conductivity of dense fibrous composites with graded interface. J. Thermophys. Heat Tr. **24**, 316-324 (2010).
DOI: https://doi.org/10.2514/1.45295

[48] C. Shen, Q. Sheng, H. Zhao, Predicting effective thermal conductivity of fibrous and particulate composite materials using convolutional neural network. Mech. Mater. **186**, 104804 (2023).
DOI: https://doi.org/10.1016/j.mechmat.2023.104804

[49] E. Ahmadloo, S. Azizi, Prediction of thermal conductivity of various nanofluids using artificial neural network. Int. Commun. Heat. Mass. **74**, 69-75 (2016).
DOI: https://doi.org/10.1016/j.icheatmasstransfer.2016.03.008

[50] W. Fei, G.A. Narsilio,M.M. Disfani, Predicting effective thermal conductivity in sands using an artificial neural network with multiscale microstructural parameters. Int. J. Heat. Mass. Tran. **170**, 120997 (2021).
DOI: https://doi.org/10.1016/j.ijheatmasstransfer.2021.120997

[51] M.A. Almomani, J.A. Hamdan, Predicting the thermal conductivity of yttria stabilized zirconia thermal barrier coatings using machine learning. Int. J. Interact. Des. Manuf. **20**, 1813-1829 (2026).
DOI: https://doi.org/10.1007/s12008-025-02451-y

[52] Y. Liu, K. Chen, A. Kumar, P. Patnaik, Principles of machine learning and its application to thermal barrier coatings. Coatings. **13**, 1140 (2023). DOI: https://doi.org/10.3390/coatings13071140

[53] H. Xia, Z.D. Sha, Predicting thermophysical properties and fracture toughness of Zirconia-based thermal barrier coating by interpretable machine learning method. Mater. Today. Commun. **46**, 112842 (2025).
DOI:https://doi.org/10.1016/j.mtcomm.2025.112842

[54] A. Lindemann, F. Beckstein, M. Brunner, Penetration Model in the NETZSCH LFA Software− Porous Materials Finally Handled Properly! https://analyzing-testing.netzsch.com/en/application-literature/penetration-model-in-the-netzsch-lfa-software-porous-materials-finally-handled-properly.

[55] K.S. Ravichandran, K. An, R.E. Dutton, S.L. Semiatin, Thermal conductivity of plasma-sprayed monolithic and multilayer coatings of alumina and yttria-stabilized zirconia. J. Am. Ceram. Soc. **82**, 673-682 (1999).
DOI: https://doi.org/10.1111/j.1151-2916.1999.tb01816.x

[56] D. Smith, S. Grandjean, J. Absi, S. Kadiebu, S. Fayette, Grain-boundary thermal resistance in polycrystalline oxides: alumina, tin oxide, and magnesia. High. Temp. – High. Press. **35**, 93-99 (2003). DOI: https://doi.org/10.1068/htjr084

[57] A. Mera, M.A. Rehman, Exploring the physical properties of Ae_2TlCoF_6 (Ae=Rb,Cs) double perovskites for solar cell applications by first-principles calculations. Inorg. Chem. Commun. **158**, 111656 (2023).
DOI: https://doi.org/10.1016/j.inoche.2023.111656

[58] A. Mera, M.A. Rehman, Z. ur Rehman, First-principles calculations to investigate the physical properties of lead-free double perovskites Cs_2AgXCl_6 (X= P, Co, As, Cd) for optoelectronic applications. Chinese. J. Phys. **87**, 268-283 (2024).
DOI: https://doi.org/10.1016/j.cjph.2023.11.005

[59] G. Moskal, L. Swadźba, M. Hetmańczyk, B. Witala, B. Mendala, J. Mendala, P. Sosnowy, Characterization of microstructure and thermal properties of $Gd_2Zr_2O_7$-type thermal barrier coating. J. Eur. Ceram. SOC. **32**, 2025-2034 (2012).
DOI: https://doi.org/10.1016/j.jeurceramsoc.2011.11.043

[60] L. Swadźba, G. Moskal, B. Mendala, T. Gancarczyk, Characterisation of APS TBC system during isothermal oxidation at 1100°C. Arch. Mater. Sci. Eng. 28, 757-764 (2007).

[61] G. Moskal, L. Swadźba, M. Hetmańczyk, B. Witala, B. Mendala, J. Mendala, P. Sosnowy, Characterisation of the microstructure and thermal properties of $Nd_2Zr_2O_7$ and $Nd_2Zr_2O_7$/YSZ thermal barrier coatings. J. Eur. Ceram. Soc. **32**, 2035-2042 (2012). DOI: https://doi.org/10.1016/j.jeurceramsoc.2011.12.004

[62] A. Jasik, G. Moskal, M. Mikuśkiewicz, A. Tomaszewska, S. Jucha, D. Migas, H. Myalska, Oxidation behavior of the monolayered $La_2Zr_2O_7$, Composite $La_2Zr_2O_7$+ 8YSZ, and double-ceramic layered La_2Zr2O_7/$La_2Zr_2O_7$+ 8YSZ/8YSZ thermal barrier coatings. Materials. **13**, 3242 (2020).
DOI: https://doi.org/10.3390/ma13143242

[63] M.J. Khan, G. Moskal, A. Iqbal, M. Mikuśkiewicz, T. Pawlik, P. Olesik, Hot corrosion behavior of single-layered $Gd_2Zr_2O_7$, $Sm_2Zr_2O_7$, and $Nd_2Zr_2O_7$ thermal barrier coatings exposed to Na_2SO_4+ $MgSO_4$ environment. Coatings. **13**, 1311 (2023).
DOI: https://doi.org/10.3390/coatings13081311

[64] S.O. Jucha, G. Moskal, Thermal barrier coatings on the base of samarium zirconates. in Production, Properties, and Applications of High Temperature Coatings. IGI Global Scientific Publishing (2018).

[65] J. Schindelin, I. Arganda-Carreras, E. Frise, V. Kaynig, M. Longair, T. Pietzsch, C. Rueden, S. Saafeld, B. Schmid, J.Y. Tinevez, D.J. White, V. Hartenstein, K. Eliceiri, P. Tomancak, A. Cardona, Fiji: an open-source platform for biological-image analysis. Nat. Methods. **9**, 676-682 (2012).
DOI: https://doi.org/10.1038/nmeth.2019

[66] G. Moskal, Selection of low and ultra-low thermal conductivity materials for insulating layers of TBC systems in the context of computational materials science opportunities – a review. J. Therm. Anal. Calorim. **150**, 7207-7251 (2025).
DOI: https://doi.org/10.2139/ssrn.4604244

[67] H.S. Yang, G.R. Bai, L.J. Thompson, J.A. Eastman, Interfacial thermal resistance in nanocrystalline yttria-stabilized zirconia. Acta. Mater. **50**, 2309-2317 (2002).
DOI: https://doi.org/10.1016/s1359-6454(02)00057-5

[68] S. Fayette, D.S. Smith, A. Smith, C. Martin, Influence of grain size on the thermal conductivity of tin oxide ceramics. J. Eur. Ceram. Soc. **20**, 297-302 (2000).
DOI: https://doi.org/10.1016/s0955-2219(99)00171-5

[69] D.S. Smith, F. Puech, B. Nait-Ali, A. Alzina, S. Honda, Grain boundary thermal resistance and finite grain size effects for heat conduction through porous polycrystalline alumina. Int. J. Heat. Mass. Tran. **121**, 1273-1280 (2018).
DOI: https://doi.org/10.1016/j.ijheatmasstransfer.2018.01.082

[70] F. Yang, X. Zhao, P. Xiao, Thermal conductivities of YSZ/Al_2O_3 composites. J. Eur. Ceram. Soc. **30**, 3111-3116 (2010).
DOI: https://doi.org/10.1016/j.jeurceramsoc.2010.07.007

[71] R. McPherson, B.V. Shafer, Interlamellar contact within plasma-sprayed coatings. Thin. Solid. Films. **97**, 201-204 (1982).
DOI: https://doi.org/10.1016/0040-6090(82)90453-9

[72] L. Lu, F.C. Wang, Z. Ma, Q.B. Fan, Anisotropic effect of splat interface on thermal conductivity of plasma sprayed YSZ coating. Surf. Coat. Technol. **235**, 596-602 (2013).
DOI: https://doi.org/10.1016/j.surfcoat.2013.08.031

[73] C.J. Li, A. Ohmori, Relationships between the microstructure and properties of thermally sprayed deposits. J. Therm. Spray. Techn. **11**, 365-374 (2002).
DOI: https://doi.org/10.1361/105996302770348754